Structural, Optical and Electrical Conductivity Studies in Polycarbazole and Its Metal Oxide Nano Composites

Sankarappa Talari (sankarappa@rediffmail.com)
Gulbarga University
B. Raghavendra
Gulbarga University
Amarkumar Malge
Gulbarga University

Research Article

Keywords: Polycarbozole, poymer nano composites, conductivity, optical absorption, band gap

Posted Date: October 26th, 2021

DOI: https://doi.org/10.21203/rs.3.rs-993638/v1

Abstract

Polycarbazole (PCz) has been synthesized by chemical oxidation method using APS as an oxidizing agent and PCz/CuO and PCz/Fe_2O_3 nanocomposites by in situ polymerization method for different wt% of CuO and Fe_2O_3 at room temperature. XRD patterns confirmed crystalline nature of samples. FTIR indicated strong interaction between PCz and nano fillers. The morphological and optical absorption studies were carried out using SEM and UV-Vis respectively. Addition of CuO or Fe_2O_3 to PCz decreased its direct and indirect band gaps. However, band gap showed a small change with dopant contents up to 30%. Urbach energy decreased with the addition of dopants. But Urbach energy of the composites increased with increasing dopants content from 10 to 30%. DC conductivity of PCz and its nanocomposites has been measured by following two probe technique in the temperature range from 300 K to 423 K. he conductivity of both the nanocomposites is found to be less than the pure PCz and it is found to increase with wt% of CuO or Fe_2O_3 as the case may be. The activation energy has been determined by fitting Arrhenius expression to the dc conductivity data at high temperature. The activation energy of polycarbazole is determined to be less than that of the composites. In both the composites, activation energy decreased and conductivity increased with the increase of dopant content.

1. Introduction

Polymers are the outstanding invention of the twentieth century which are of long chain structure and generally shows insulating behavior. Conducting polymers are a group of polymers which conduct electricity in pure and doped forms. Conducting polymers are extensively used in manufacturing of sensors, solar cells, diodes, electrochemical super capacitors, memory storage devices, actuators and corrosion protection [1–7].

Recently, the conductivity of many conducting polymers doped with metal oxides have been widely investigated. Among these, polycarbazole (PCz) has been captivated more by its superior properties such as good electrical and thermal, conductivity, high hole mobility, low redox potential and feasible molecular structure and tuning properties [8]. Ahmad Zahoor et al [9] have fabricated Ag/PCz by microwave polyyol reduction method. Through FTIR and Raman measurements they observed that Ag nanoparticles are enclosed by 3,6 polycarbazole. It was concluded that these composites are advantageous to combine the luminescence behavior of Ag nanopartiles and PCz. Umair Baig et al [10], studied DC conductivity of PCz/ZrP and reported increase in resistivity on exposure to ammonia, at room temperature. Aditi Srivatsva et al [11] have fabricated a p-Polycarbazole/n-ZnO hybrid heterojunction diode and reported that it exhibits low dark current in the range of 10^{-11} A.

The electrical and optical properties of a conducting polymer could be altered by doping metal oxides to it. There have been many studies reported on metal oxide doped polymer nanocomposites with dopants such as CuO, ZnO, Cu_2O, MnO_2, ZrO_2,TiO_2 and SnO_2 [12–18]. Copper Oxide is blackish brown in color and has monoclinic structure. The manufacturing cost of CuO is vary less, shows semiconducting nature and

measure a small band gap. S. Ashokan et al [19] have studied conducting properties and sensing properties of PANI/CuO nanocomposites. G. Rajasudha et at [20] have synthesized polyindole-CuO nanocomposite by sol gel method and studied temperature dependent conductivity of polyindole/CuO nanocomposite. Polypyrrole-CuO nano composites were prepared by khan Malook et al. They observed that the incorporation of different concentration of CuO to polypyrrole decreases the energy band gap of polypyrrole [21]. Fe_2O_3 is an inorganic n-type semiconductor shows a nontoxic behavior, which can be abundantly obtained in nature. Fe_2O_3 is considered as a good electrode material used for constructing lithium ion batteries. R. Gangopadhyaya et al [22] have prepared polypyrrole/Fe_2O_3 naocomposites and studied conductivity. They noted variations in both ac and dc conductivity for different concentration of Fe_2O_3.

In view of the fact that there are no many reports on PCz and its composites, we synthesized and investigated polycarbazole, PCz/CuO and PCz/Fe_2O_3 nanocomposites for structural, morphological, optical and electrical properties. Results have been analyzed and presented in this article.

2. Experimental

2.1 SAMPLE PREPARATION

The materials used are carbazole (Sigma-Aldrch), acetonitrile (SD-Fine), Ammonium persulfate, (SD fine), Acetone (Merck), CuO (HIMEDIA), Fe_2O_3 (HIMEDIA), nanoparticles and deionised water are of analytical grade.

SYNTHESIS OF PCz

The PCz was synthesized by chemical oxidative polymerization method. Monomer solution was prepared by dissolving 3.34 gm of Carbazole in 50ml of acetonitrile. The APS (oxidant) solution was prepared by dissolving 9.12gms of APS in 50ml of water. Molar ratio of 1:2 was maintained between monomer and oxidant. The APS solution was added slowly (drop wise) to the carbazole solution over a period of 30 min. The mixture was constantly stirred for 24 hours at room temperature and obtained dark green solution. The precipitate was filtered and washed several times with deionised water and methonal and kept the yield for annealing at 150̊ C.

SYNTHESIS OF PCz/CuO AND PCz/Fe_2O_3 COMPOSITES

The nanocomposites were prepared by in situ oxidative polymerization of carbazole by adding different amounts of CuO using APS as oxidizing agent. Carbazole (3.34gms) was dissolved in acetonitrile (50ml). CuO (10 wt%) nanoparticles was added to monomer solution under vigorous stirring. APS solution (9.12gms in 50ml of water) was added drop wise to the above solution over a period of 15 minutes. The entire solution was stirred for 24 and the color of the solution turned to dark green. The precipitate was washed several times with deionised water and methanol successively, filtered and then dried. PCz/Fe_2O_3

nanocomposites of different wt% of Fe_2O_3 were synthesized by following the same procedure. The different concentrations of CuO and Fe_2O_3 (10, 20, 30 wt%) were prepared and labeled as PCu10, PCu20, PCu30 and PFO10, PFO20 and PFO30 respectively.

2.2 MEASUREMENTS

The powder XRD experiments were performed on all the samples using Cu-Kα radiation of wavelength 1.5405Å in a Rigaku Ultima IV diffractometer. SHIMADZUIR-Prestige-21 Fourier transform infrared spectrophotometer was used to acquire FTIR spectra of the samples in the wave number range of 400–4000 cm^{-1}. UV–Visible spectra were recorded using UV Visible1899 spectrometer for the wavelength range 200–900 nm. The samples which are in powder form were pelletized in a hydraulic press by applying the pressure of 20 kg/cm^2. The dc conductivity measurements were carried out by applying a constant voltage of 5 V across the pellet in the temperature range from 300 K to 423 K by employing a two probe method. Current was measured using a nano ammeter. The electrical resistivity, ρ was estimated by ρ = R(A/t), where R = (V/I), A is area of cross section and t the thickness of pellet. Conductivity, σ has been determined using the expression, σ = 1/ρ, within the accuracy of 2%.

3. Results And Discussion

3.1 XRD

The crystalline structure of pure PCz and composites PCz/CuO and PCz/Fe_2O_3 were investigated from XRD patterns. The XRD patterns of the present samples are shown in the below Fig. 1. Some diffraction peaks corresponding to different crystalline planes can be seen. The sharp peaks at 35.77, 38.91, 48.82, 53.54, 58.54, 61.62, 66.50, 68.18, 72.59, 75.35 correspond to (0 0 2), (2 0 0), (2 0 2), (0 2 0), (2 0 2), (1 1 3), (0 0 2), (2 2 0), (3 1 1), (0 0 4) planes of monoclinic structure of CuO. Peaks at 24.19, 33.15, 35.77, 40.96, 49.68, 54.32, 62.47, 63.96 correspond to (0 1 2), (1 0 4), (1 1 0), (1 1 3), (0 2 4), (1 1 6), (2 1 4), (3 0 0) planes of rhombohedral structure of Fe_2O_3. The CuO and Fe_2O_3 patterns are found to be consistent with JCPDS file Nos. 48-1548 and 89-8104 respectively [19, 23]. The peaks at 19.03, 20.01, 21.16, 23.16, 28.12 correspond the planes (2 0 -1), (1 2 -1), (2 2 0), (0 1 2), (2 1 0) of polycarbazole [24]. The increase in peak intensity with increasing concentration of CuO and Fe_2O_3 confirms interaction of dopants with PCz. The crystallinity of the composites enhanced due to increased concentration of nano sized dopants.

The crystallite size, D was determined from XRD patterns using Debye Scherer's formula showed in Eqn (1) and micro strain, ε using Eqn (2) [25],

$$D = \frac{K\lambda}{ß Cos\theta} \quad (1)$$

$$\varepsilon = \frac{ß}{4tan\theta} \quad (2)$$

Where, K is a constant called shape factor equal to 0.9 for spherical shaped particles [24], λ is wavelength of X-ray (1.5406Å), ß is full width half maximum and θ position of the peak. The prominent peak for each sample was considered for determining crystallite size and micro strain. The obtained values of crystallite size, average crystallite size and micro strain of the samples are tabulated in Table 1. It can observed that the crystallite size of PCz is less compared to composites, crystallite size is increasing and micro strain is decreasing with wt% of dopants which confirms encapsulation of polycarbazole on the dopant particles. These are in qualitative agreement with the literature on PCz/SnO_2 [24].

Table 1
Crystallite size, D average crystallite size and Micro strain, ε of PCz, PCuO and PFO composites.

Sl no	Sample	2θ (Degrees)	FWHM (ß)	Crystallite size (nm)	Average crystallite size (nm)	Micro strain (ε)
1	PCz	20.04	0.33	24.07	24.07	0.47
2	CuO	35.60	0.27	29.42	29.42	
3	Fe_2O_3	33.35	0.31	25.62	25.62	
4	PCu10	19.43	0.30	26.51	34.14	0.44
5	PCu20	19.53	0.25	31.77		0.36
6	PCu30	19.52	0.18	44.15		0.26
7	PFO10	19.49	0.26	30.06	42.89	0.38
8	PFO20	19.51	0.19	41.81		0.27
9	PFO30	19.47	0.14	56.82		0.20

3.2 FTIR ANALYSIS

The FTIR has been analyzed to know different functional groups developed in the composites due to interaction between constituents such as PCz and CuO and, PCz and Fe_2O_3. The spectra of the present nanocomposites are shown in the Fig. 2. The IR bands at 726cm^{-1} and 812 cm^{-1} are due to C-H deformation of di-substituted and tri-substituted benzene ring of PCz respectively [26, 27]. A sharp band around 3415cm^{-1} refers to stretching of the N-H bond in PCz. The change in intensity and shifting of 3415cm^{-1} band evidenced the formation of bond between NH group of PCz and CuO and, Fe_2O_3 [25]. The presence of the stretching band at 1227 cm^{-1} is attributed to C=N and the peak at 1316 cm^{-1} is attributed to C-H out of plane bending vibration of aromatic ring. The sharp band at 1444 cm^{-1} may be due to ring stretching vibration of carbazole [27]. The bands at 918 cm^{-1} and 1598 cm^{-1} are assigned to =CH out of plane and stretching mode of aromatic alkene respectively [21, 25]. A strong absorption band at 562 cm^{-1}

and at 602 cm^{-1} in the composites confirms incorporation of Cu-O and Fe-O vibrational modes respectively [21, 23]. The assignment of bands of different fuctional groups are tabulated in Table 2.

Table 2
Assignment of bands to different functional groups in FTIR spectra of PCz, PCuo and PFO composites.

S.No	FTIR bands in PCz (cm^{-1})	FTIR bands in PCz/CuO composites (cm^{-1})	FTIR bands in PCz/Fe_2O_3 composites (cm^{-1})	Assignment of bands
1			562-563	Fe-O stretching vibratio mode[23]
2		602 To 610		Vibration of Cu-O bond[21]
3	726	717 To 723	720	Ring deformation of substituted aromatic structure[26]
4	812	812	814	C-H deformation in tri substituted benzene ring[27]
5	918	918	918	= CH out of plane vibrations[21]
6	1227	1227	1232	C=N stretching[27]
7	1316	1316	1316	C-H out of plane bending vibration of aromatic ring[27].
8	1444	1444	1444	Ring stretching vibration of carbazole moiety[27].
9	1598	1598	1598	stretching mode of aromatic alkene [25]
10	3415	3415-3419	3415-3420	Stretching of N-H bond [25]

3.3 MORPHOLOGY

Figure 3 show3.3 MORPHOLOGYs typical SEM images of PCz, PCu10 and PFO10 nanocomposites. It is evident from the images that the polycarbazole has homogeneous surface morphology with nodular nature and the particles are agglomerate. It can be observed from the images of the PCz/CuO, PCz/Fe_2O_3 nanocomposites the morphological changes occurring upon adding the CuO/Fe_2O_3 nanoparticles. The added nanofillers lead to branching of polymer chain in the polycarbazole and that intern create network like structure in composites, Polycarbazole in PFO composites.

3.4 UV-VIS ABSORPTION ANALYSIS

Figure 4 (a & b) depicts optical absorption spectra of the samples PCz, PCu10, PCu20, PCu30, PFO10, PFO20 and PFO30. A broad band is observed at 279nm in pure polycarbazole is assigned to bonding and antibonding (π-π*) transition of the benzoid ring and small peak around 347nm is corresponding to polaronic energy level (n-π*) transition of the quinoid ring. The polaronic energy level is created by the formation of defects during polymerization process [24, 26]. It is observed that the peaks are slightly shifted to blue end about 4nm for CuO composites and to 8nm for Fe_2O_3 composites of spectrum and also there is variation in the intensity with different concentration of CuO and Fe_2O_3. This is because CuO or Fe_2O_3 nanoparticles absorbs partly incident radiation by their free electrons and due to the strong interaction between polymer and dopant nanopartiles. The blue shift on a small scale with increase in CuO wt% is in agreement with the reports, PCz/SnO_2 [25].

The optical absorption gives information about band gap and electronic transitions. Optical energy gaps can be determined using Mott-Davis-Tauc's equation [28].

$(\alpha h\nu)^{1/n} = \frac{2.303}{d} = B\,(h\nu - E_g)$ (3)

Where, α is the absorption coefficient, B the absorption constant, *hv* the energy of the photon, E_g the optical energy gap and d the sample thickness. The exponent (1/n) represents different electronic transitions and it takes values $\frac{1}{2}$, 2, $\frac{3}{2}$ and 3 corresponding to allowed direct, indirect, forbidden direct and forbidden indirect transitions respectively. The direct and indirect energy gaps are determined from the transition of electrons from valance band to conduction band when photons interact with them in the valance band.

The Tauc's plots for direct and indirect transitions were made and tangents to the band edges were extrapolated on to the *hv*-axis. The intersecting values on *hv*-axis gave band gap values corresponding to direct or indirect transitions as the case may be. The typical plots of direct band gap for one sample in each series and for pure PCz are shown in Fig. 5 and for indirect band gap in Fig. 6. To save space, Tauc's plots for all the corresponding are not shown in the Fig. 5 & 6.

The results tabulated in Table 3 revealed that the intended direct and indirect band gap values of pure PCz were 3.32 eV and 3.42 eV respectively. For PCu10, direct and indirect gaps are found to be 3.47eV and 3.54 eV respectively. It implies that band gap values increases on doping PCz with CuO. Similarly, for PFO10, direct and indirect gaps are 3.49 eV and 3.53 eV. These results are also suggest that band gap of PCz increases when doped with Fe_2O_3. This may be due to strong interaction between the polymer matrix and dopant oxides. Increase of CuO or Fe_2O_3 from 10 wt% to 30 wt% decreases band gaps slightly. Similar nature of results were reported for PCz/SnO_2 and PVA/CuO [24, 28].

Table 3
Optical Band gap energy (direct and indirect) and Urbach energy values for PCz, PCuo and PFO composites.

Sl no	Sample	Direct band gap E_g (eV)	Indirect band gap E_g (eV)	Urbach energy E_u (eV)
1	PURE PCz	3.32	3.42	0.32
2	PCu10	3.47	3.54	0.30
3	PCu20	3.48	3.53	0.31
4	PCu30	3.46	3.52	0.32
5	PFO10	3.49	3.53	0.30
6	PFO20	3.47	3.52	0.32
7	PFO30	3.46	3.51	0.33

The Urbach energy (E_u) was determined by plotting ln(α) versus *hv* as depicted in Fig. 7. Urbach energy (E_u) of pure PCz is determined to be 0.325 eV [Table 3]. This value decreased to 0.307 eV when 10 wt% of CuO or Fe_2O_3 are doped to PCz. Since Urbach energy is a measure of defects in the sample, present results indicate that samples improve their quality in terms of defects when they were doped with 10 wt% of dopant oxides. On increasing dopants beyond 10 wt% Urbach energy increases. This reveals that higher amounts of dopant oxides increases concentration of structural defects in the samples. Similar results were quoted for PVA/CuO composits [28].

3.5 CONDUCTIVITY

Conductivity, σ of pure PCz and the composites is observed to be increasing with increase of temperature and is of the order of 10^{-5} $(\Omega m)^{-1}$. This reveals semiconducting behavior of the samples. In composites, conductivity increased with increase of CuO or Fe_2O_3 contents. Conductivity of the composites is found to be less than that of pure PCz at all the temperatures of interest. Increase in conductivity with increase in CuO/Fe_2O_3 concentration may be due to formation of well organized network for transportation of charge carriers by the added dopants. Raj et al studied temperature dependent conductivity of pure PCz and their conductivity was in the order of 10^{-5} $(\Omega m)^{-1}$[26].

The temperature variation of electrical conductivity is analyzed using Arrhenius expression,

$\sigma = \sigma_0 \exp(E_a/k_BT)$ (4)

Where, σ is conductivity, E_a the activation energy and k_B the Boltzman constant.

Figure 8 and Fig. 9 shows the plots of ln(σ) versus (1/T) for pure PCz and PCuO and PFO composites respectively. The linear lines were fit to the data at higher temperatures and the obtained slopes of the fits were used to determine the activation energy E_a. Fig. 10 shows activation energy (E_a) and σ at 400 K versus wt% of CuO/Fe_2O_3 composites, it can be seen that activation energy E_a decreased and conductivity increased with increase of dopant concentration and, it may be due to the decrease in the scattering rate of polarons with increase of CuO/Fe_2O_3 concentration. The conductivity and activation energy values of PCz, PCz/CuO and PCz/Fe_2O_3 nanocomposites at 350 K and 400 K are tabulated in Table 4. To emphasize conductivity behavior with filler content its value at two different temperatures are shown in Table 4. Similar kind of behavior in E_a and σ has been observed by J. Selvi et al [29] for PVA/CuO composites and noticed enhancement in conductivity and reduced activation energy in PVA doped CuO. Mohammad Shakir et al [30] have noticed increase in conductivity with TiO_2 content in PCz/TiO_2 nanocomposite. Syed Abthagir et al [31] compared conductivity of polyindole, polycarbazole and their derivatives and found that polycarbazole had higher conductivity than polyindole.

Table 4
DC conductivity, σ at 350 K and 400 K and activation energy, E_a for conduction for PCz and PCuO and PFO composites .

sl no	Sample	E_a (meV)	σ (350 K) $(\times10^{-5})\ (\Omega m)^{-1}$	σ (400 K) $(\times10^{-5})\ (\Omega m)^{-1}$
1	PCz	4.91	3.19	3.26
2	PCu10	15.11	1.95	2.07
3	PCu20	8.29	2.07	2.13
4	PCu30	7.25	2.45	2.55
5	PFO10	8.68	1.20	1.25
6	PFO20	8.42	1.80	1.83
7	PFO30	5.99	2.22	2.27

Conclusions

In the present work, polycarbazole has been synthesized via chemical oxidation method and the composites, PCz/CuO and PCz/Fe_2O_3 by in situ polymerization technique. The samples were characterized by XRD, FITR, SEM and UV-Vis. The results revealed that the composites are influenced by the loaded CuO/Fe_2O_3 nanofillers. Crystalline nature of the materials and strong interaction between PCz and dopants are confirmed by XRD and FTIR respectively. SEM images showed a remarkable morphological distinction between the polycarbazole and the composites. The optical absorption bands showed blue shifts in the peak positions which reveals inter molecular interactions between the added nanofillers and the polymer matrix. The direct and indirect band gaps were determined by Mott-Davis

Tauc equation and found that the band gap of the composites are higher than the pure polycarbazole and the band gaps of the composites showed a small change with dopant content up to wt 30% with increase in wt% of the fillers. Conductivity of both PCz and the composites increased with increase in temperature indicating semiconducting nature. conductivity of the composites increased and activation decreased with wt% of CuO/Fe_2O_3 content. For the first time PCz and its metal oxides doped composites have been thoroughly investigated for structural, morphological, optical and electrical conductivity.

References

1. M.C. Santos, O.H.C. Hamdan, S.A. Valverde, E.M. Bianchi, Synthesis and characterization of V_2O_5/PANI thin films for application in amperometric ammonia gas senors, 65, (2019) 116–120, https://doi.org/10.1016/j.orgel.2018.11.013
2. K.M. Zaidan, H.F. Hussein, R.A. Hassan, Synthesis and characterization of (Pani/n-si) solar cell. Energy procedia **6**, 85–91 (2011). https://doi.org/10.1016/j.egypro.2011.05.010
3. M. Gokcen, T. Tunc, S. Altindal, I. Uslu, Electrical and photocurrent characteristics of Au/PVA (Co-doped)/n-Si Photoconductive diodes, Materials Science and Engineering:B 177, 5, (2012) 416-420, https://doi.org/10.1016/j.mseb.2012.01.004
4. B. Muthulakshmi, D. Kalpana, S. Pitchumani, N.G. Renganathan, Electrochemical deposition of polypyrrole for symmetric supercapacitors, Journal of power sources, 158, 2, (2006) 1533-1537, https://doi.org/10.1016/j.jpowsour.2005.10.013
5. P. Burgmayer, R.W. Murray, Faster ion gate membranes, J.Electroanal,chem.,147, (1983) 339–344, https://doi.org/10.1016/S0022-0728(83)80080-1
6. J.M. Sansinena, J. Gao, H.L. Wang, High-performance, Monolithic polyaniline Electrochemical Actuators, Advanced Functional Materials, 13, 9, (2003) 703-709, **https://doi.org/10.1002/adfm.200304347**
7. S.T. Doslu, B.D. Mert, B. Yazici, Polyindole top coat on TiO_2 sol-gel films for corrosion protection of steel. Corrosion Sciene colume **66**, 51–58 (2013). https://doi.org/10.1016/j.corsci.2012.08.067
8. LuO.M. Chan Qi, P. Hemmershoj, D. Zhou, Y. Han, B. Laursen, C.G. Yan, B. Han, Micro porous polycarbazole with high specific surface area for gas storage and separation. J.Am.Chem.Soc **134**, 6084–6087 (2012). https://doi.org/10.1021/ja300438w
9. T. Ahmad Zahoor, J. Qiu, Zhang, Synthesis and characterization of Ag@polycarbazole nanopaticles and their novel optical behavior. J.Mater Sci **44**, 6054–6059 (2009). DOI 10.1007/s10853-009-3831-y
10. A. Umair Baig, Waseem, L. Wani, T. Hun, Facile synthesis of electrically conductive polycarbazole-zirconium(IV)phosphate cation exchange nanocomposite and its room temperature ammonia sensing performance. New J, Chem **20**, 1–27 (2015). DOI:10.1039/C5NJ01029B
11. P. Aditi Srivatava, Chakrabarti, Fabrication and electrical characterization of a polycarbazole/ZnO based Organic and inorganic hybride heterojunction diode. superlattices and Microstructures **88**, 723–730 (2015). Doi:org/10.1016/j.spmi.2015.10.035

12. L.N. Shubha, P. Madhusudana Rao, Temperature characterization of dielectric permittivity and AC conductivity of nano copper oxide- doped polyaniline composite, 6, 3, (2016) 1650018–1650025, DOI:10.1142/S2010135X16500181
13. A.M. El Sayed, W.M. Morsi, α-Fe_2O_3/(PVA + PEG) Nanocomposite films; synthesis, optical, and dielectric characterizations. J.Mater Sci **49**, 5378–5387 (2014). DOI 10.1007/s10853-014-8245-9
14. Y. Jianghao, MinLi,H. Wang, X. Lian, Y.F.Z. Xie, B. Niu, Wenfeng Li, preparation and property studies of chitosan-PVA biodegradable antibacterial multiplayer films doped with Cu_2O and nano-chitosan composites. Food control **126**, 108049 (2021). Doi.org/10.1016/j.foodcont.2021.108049
15. J. Zhang, D. Shu, T. Zhang, H. Chen, H. Zhao, Y. Wang, Z. Sun, Shaoqing,Tang, Xueming Fang, Xi Ufang Cao, Capacitive properties of PANI/MnO2 synthesized via simultaneous-oxidation route. Jouranal of Alloys and Compounds **532**, 1–9 (2021). Doi.org/10.1016/j.jallcom.2012.04.006
16. A. De, A. Das, S. Lahiri, Heavy ion irradiation on conducting polypyrrole and ZrO_2-polypyrrole nanocomposites. Synth. Met. **144**(3), 303–307 (2004). Doi.org/10.1016/j.synthmet.2004.04.006
17. M.O. Ansari, F. Mohammad, Thermal stability, electrical conductivity and ammonia sensing studies on p-toluenesulfonic acid doped polyaniline:titanium dioxide(pTSA/Pani:TiO2) nanocomposites. Sens. Actuators B **157**, 122–129 (2011). Doi.org/10.1016/j.snb.2011.03.036. 1
18. P. Manivel, S. Ramakrishnan, K. Nikhil, A. Kothukar.N. Balamurugan.Ponpandian, D.Mangalaraj, C..Viswanathan, Optical and electrochemical studies of polyaniline/SnO2 fibrous nanocomposites, Materials Research Bulletin, 48, 2, (2013) 640-645, doi.org/10.1016/j.materresbull.2012.11.033
19. S. Ashokan, P. Jayamurugan, V.Ponnuswamy, Effects of CuO and Oxidant on the Morphology and Conducting Properties of PANI:CuO Hybrid Nanocomposites for Humidity Sensor Application, Polymer Science, 2019,61,86-97
20. G. Rajasudha, L.M. Jayan, D. Durga Lakshmi, P. Thangadurai, Nikos –Boukos, V. Narayanan, A. Stephen, Polyindole-CuO composite polymer electrolyte containing $LiClo_4$ for lithium ion polymer batteries, Polym. Bull. (2012) 68:181–196, DOI 10.1007/s00289-011-0548-1
21. M. Khan Malook, Ihsan-ul-Haque, Khan, Muhammed ali, Polypyrrole-Cuo based composites, promotional effects of CuO contents on polypyrrole characteristics. Journal of Material Science: Materials in Electronics **30**, 3882–3888 (2019). Doi.org/10.1007/s10854-019-00673-x
22. R. Gangopadhyaya, A. De, S. Das, Transport properties of polypyrrole-ferric oxide condcucting nanocomposite. Jouranl of applied physics **87**, 2363 (2000). https://doi.org/10.1063/1.372188
23. D. Rajasudha Ganesan, N. Dhinasekaran, Thangadurai, Paramasivam, Boukos, Narayanan Vengidusamy, and Stephen arumainathan, Preparation and Characterizaton of Polyindole-Iron Oxide composite Polymer Electrolyte Containing $LiClO_4$. Polymer-Plastics Technology and Engineering **51**, 225–230 (2012). doi.org/10.1080/03602559.2011.618159
24. N.C. Horti, M.D. kamatagi, N.R. Patil, S.K. Nataraj, S.A. Patil, S.R. Inamdar, Synthesis and photoluminescence properties of polycarbazole/tin oxide (PCz/SnO_2) polymer nanocomposites. Polym. Bull. (2020). https://doi.org/10.1007/s00289-020-03428-5

25. S. Madhurima Das, Roy, Preparation, characterization and Properties of Newly Synthesized SnO_2 – Polycarbazole Nanocomposite via Room Temperature solution phase synthesis Process, Materials Today: Proceedings, 18, (2019) 5438–5446, https://doi.org/10.1016/j.matpr.2019.07.573
26. V. Raj, D. Madeswari, M. Mubarak Ali, Journal of applied science, Chemical Formation, Characterization and Properties of Polycarbazole, 116, 147-154 (2010), **https://doi.org/10.1002/app.31511**
27. A. Kumar, M. Tiwari, R. Prakash, Electrochemical Study of Interfacially Synthesized Polycarbazole with Different Oxidants, ChemElectroChem, 2, (2015) 2001 – 2010 DOI: 10.1002/celc.201500318
28. M.A. Muhammaad Aslam, Z.A. Kalyar, Raza, Fabrication of nano-CuO-loaded PVA composite films with enhanced optomechanical properties, Polymer Bulletin, https://doi.org/10.1007/s00289-020-03173-9
29. J. Selvi, S. Mahalakshmi, V. Parthasarathy, Y.-F. Vhechia Hu, K.-L. Lin, R. Tung, A.A. Anbarasan, Annie, Optical, Thermal, Mechanical Porperties, and Non-Isothermal Degradation Kinetic Studies on PVA/CuO Nanocomposites, 40, 9, (2019) 3737-3748, **https://doi.org/10.1002/pc.25235**
30. M.S. Mohammad Shakir, Noor-e-Iram, S.I. Khan, A.A. Al-Resayes, Khan, U. Baig, E. Conductivity, Isothermal Stability, and Ammonia-Sensing Performance of Newly Synthesized and Characterized Organic–Inorganic Polycarbazole–Titanium Dioxide Nanocomposite. Ind. Eng. Chem. Res. **53**, 8035–8044 (2014). dx.doi.org/10.1021/ie404314q
31. P. Syed Abthagir, R. Saraswathi, Charge transport and thermal properties of polyindole, polycarbazole and their derivatives, Thermochimica Acta, 424, 25-35 (2004), Doi.10.1016/j.tca.2004.04.028

Figures

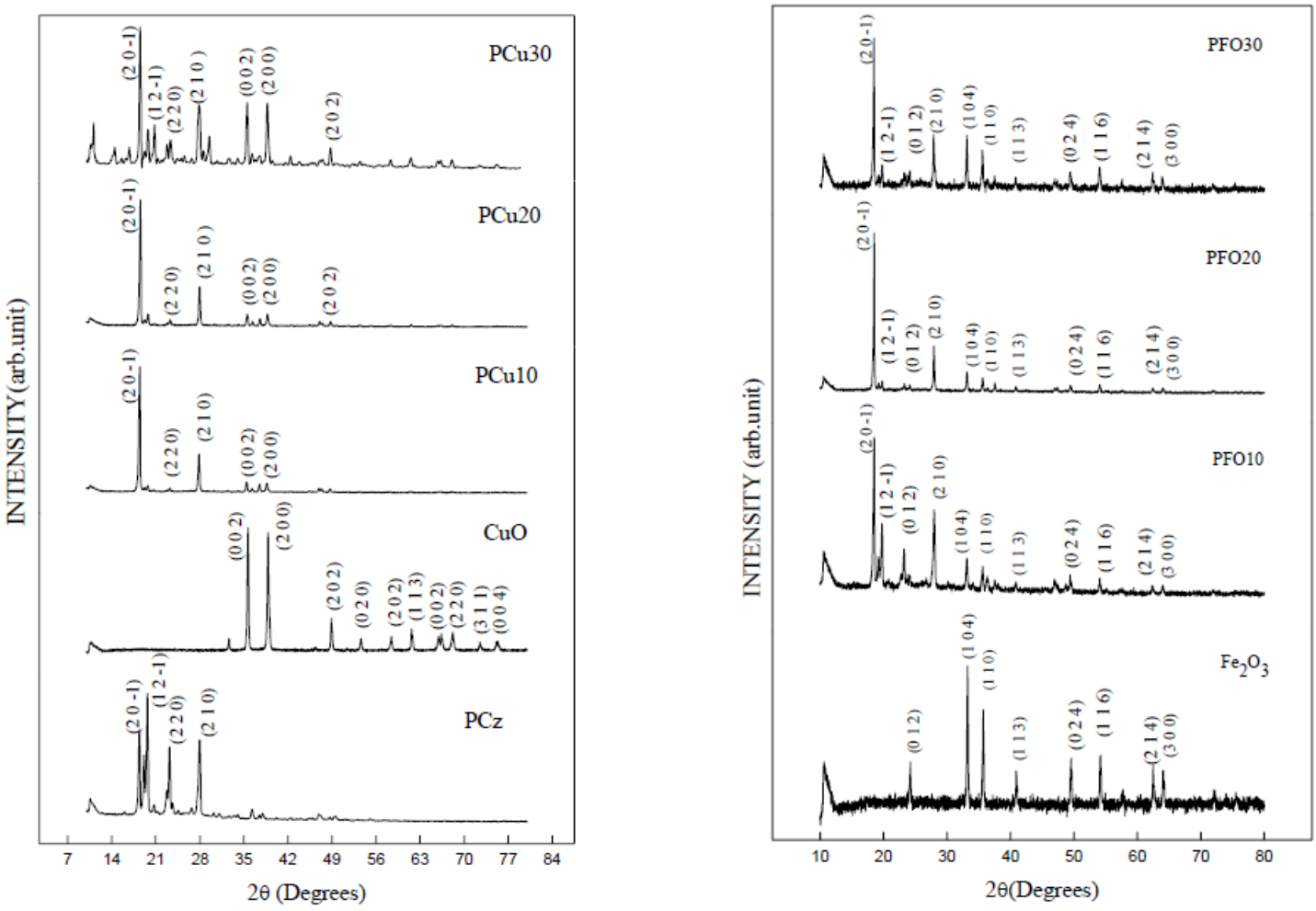

Figure 1

XRD pattern of CuO, Fe2O3, PCz, PCuO and PFO nanocomposites.

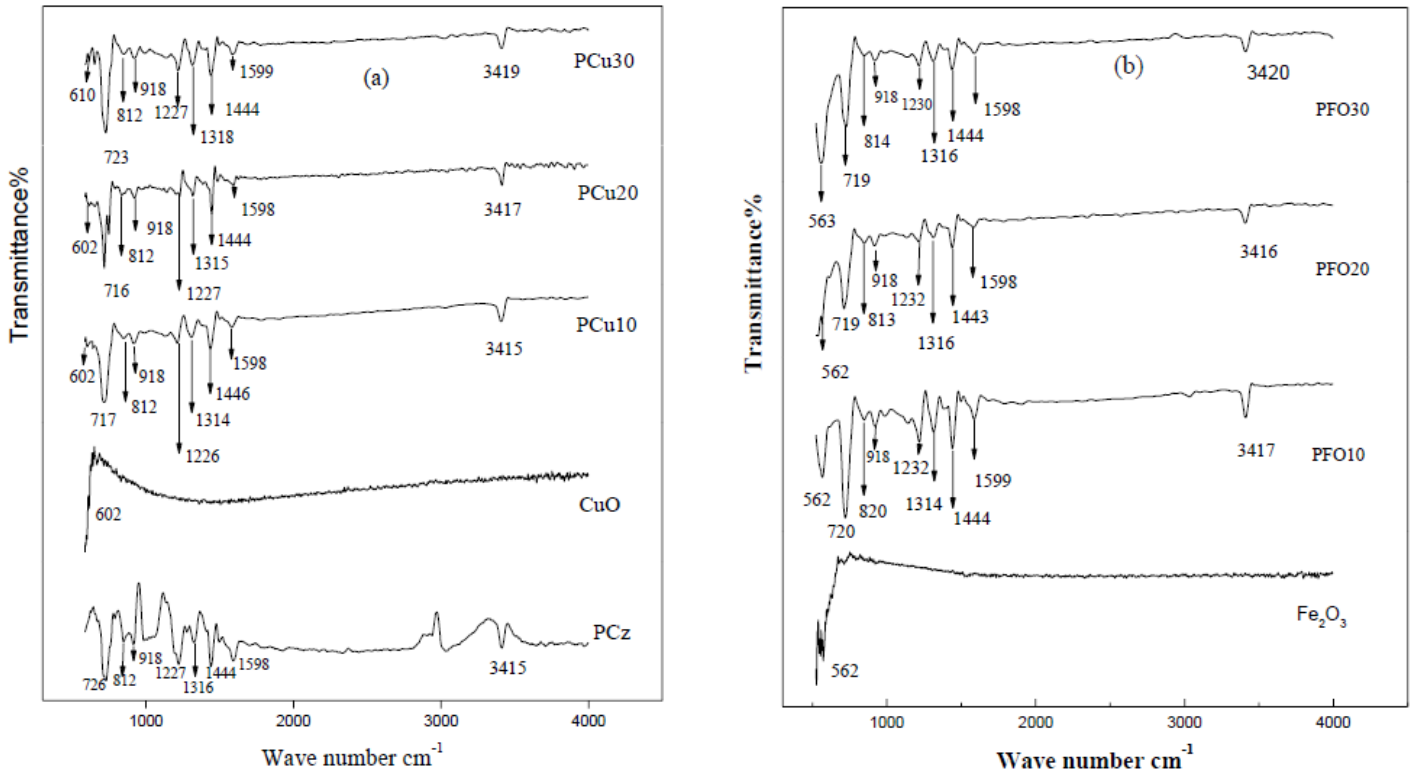

Figure 2

FTIR spectra of (a) PCz, CuO and, PCuo and, (b) Fe2O3 and PFO composites

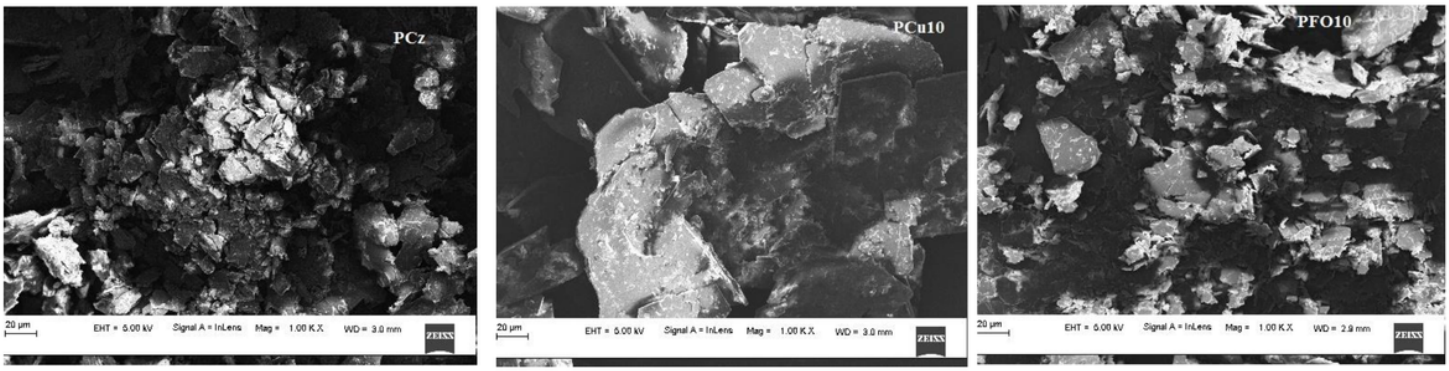

Figure 3

SEM morphologies of PCz, PCu10 and PFO10

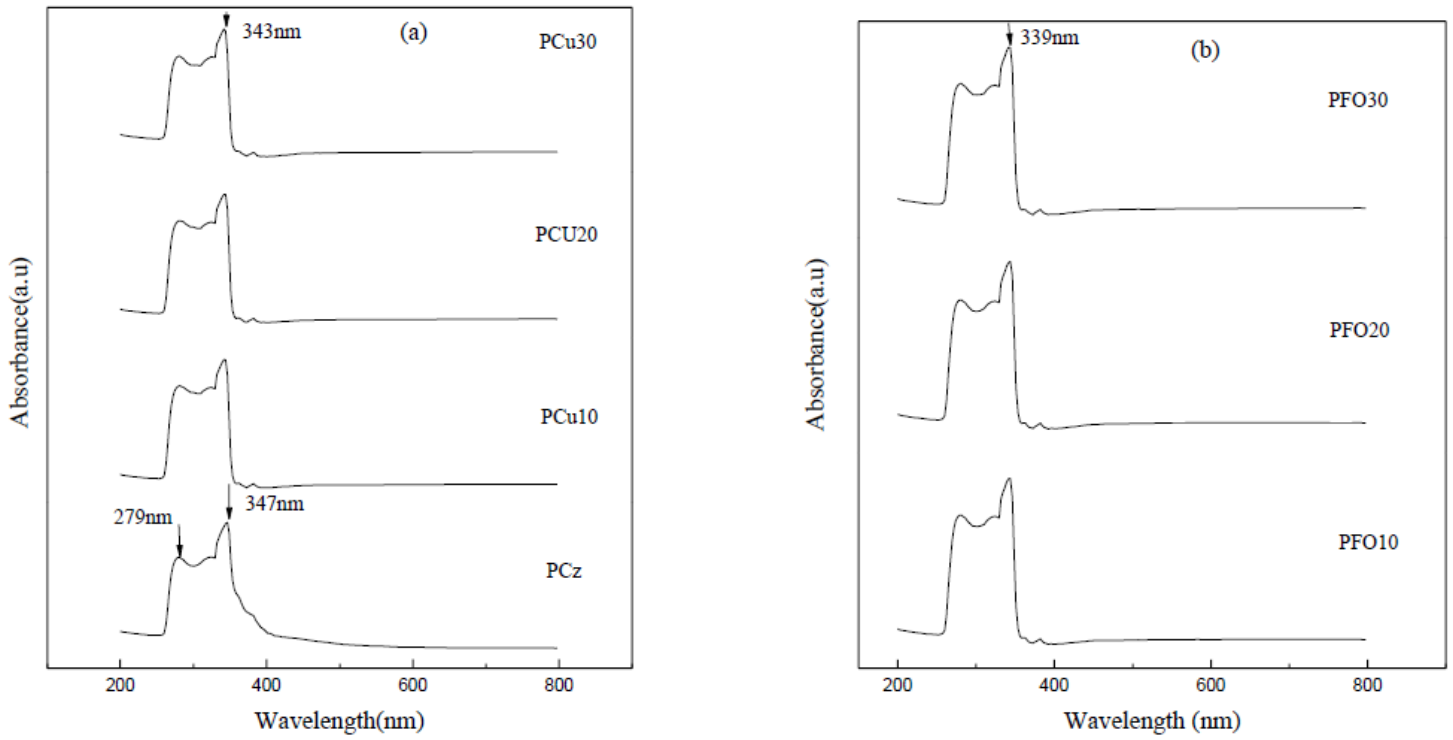

Figure 4

Optical absorbance versus wavelength for PCz and (a) PCz/CuO and (b) PCz/Fe2O3 composites

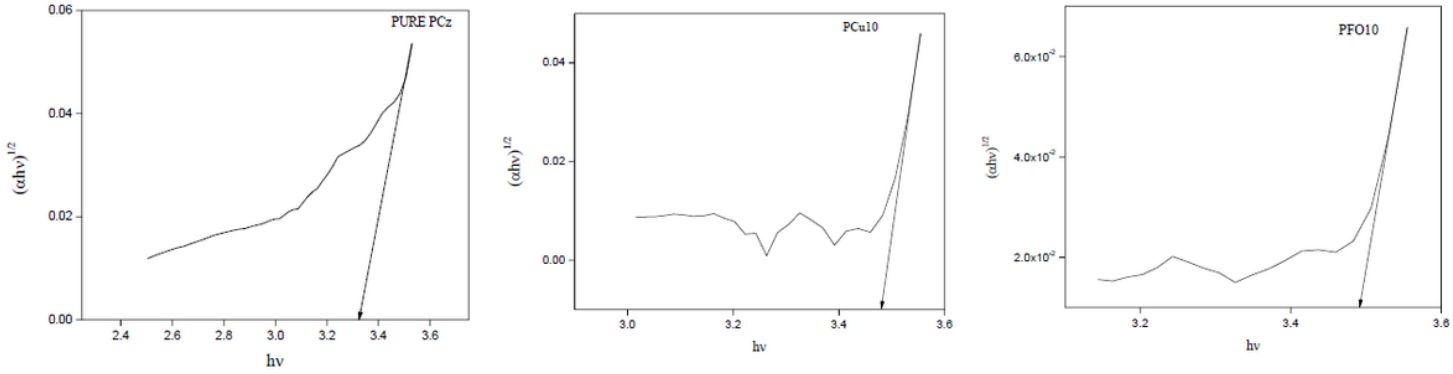

Figure 5

Tauc's plots of (αhv)1/2 versus hv for direct band gap determination.

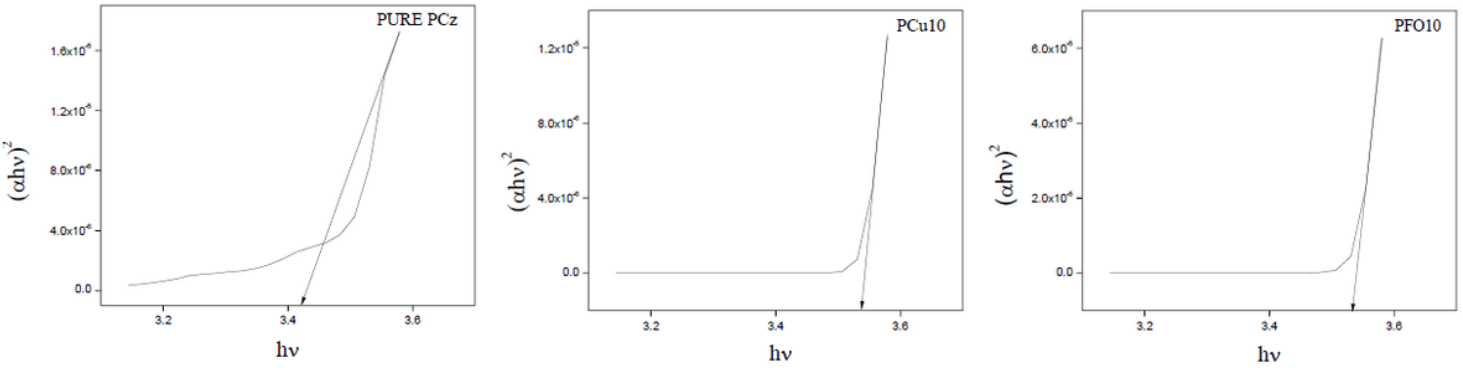

Figure 6

Tauc's plots of (αhv)2 versus hv for indirect band gap determination

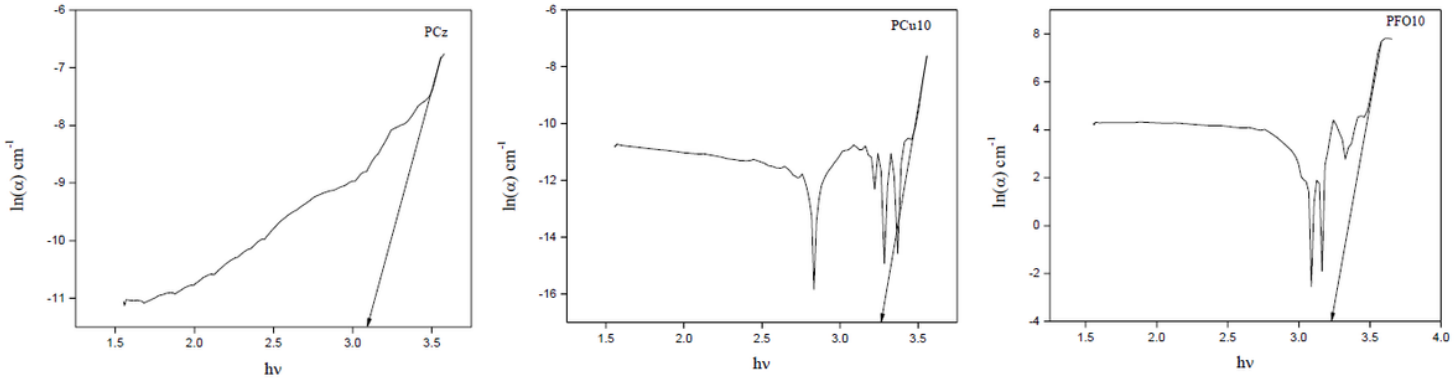

Figure 7

Plots of ln(α) versus hv for PCz, PCu10 and PFO10 composites for Urbach energy determination.

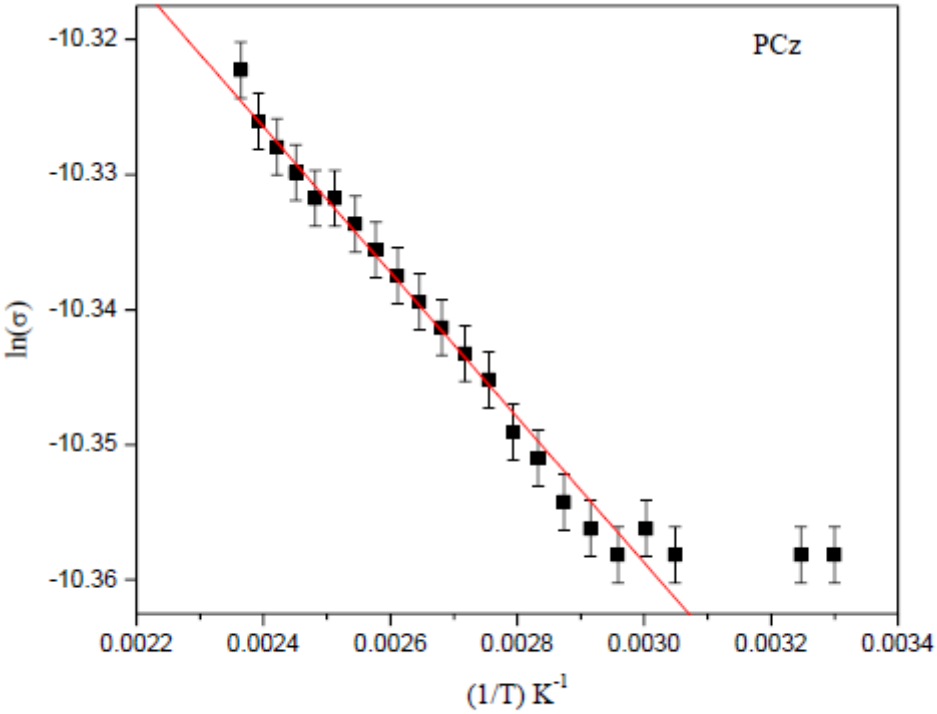

Figure 8

Plot of (ln(σ) versus 1/T) for PCz. Solid line is a linear fit to the data at high temperature.

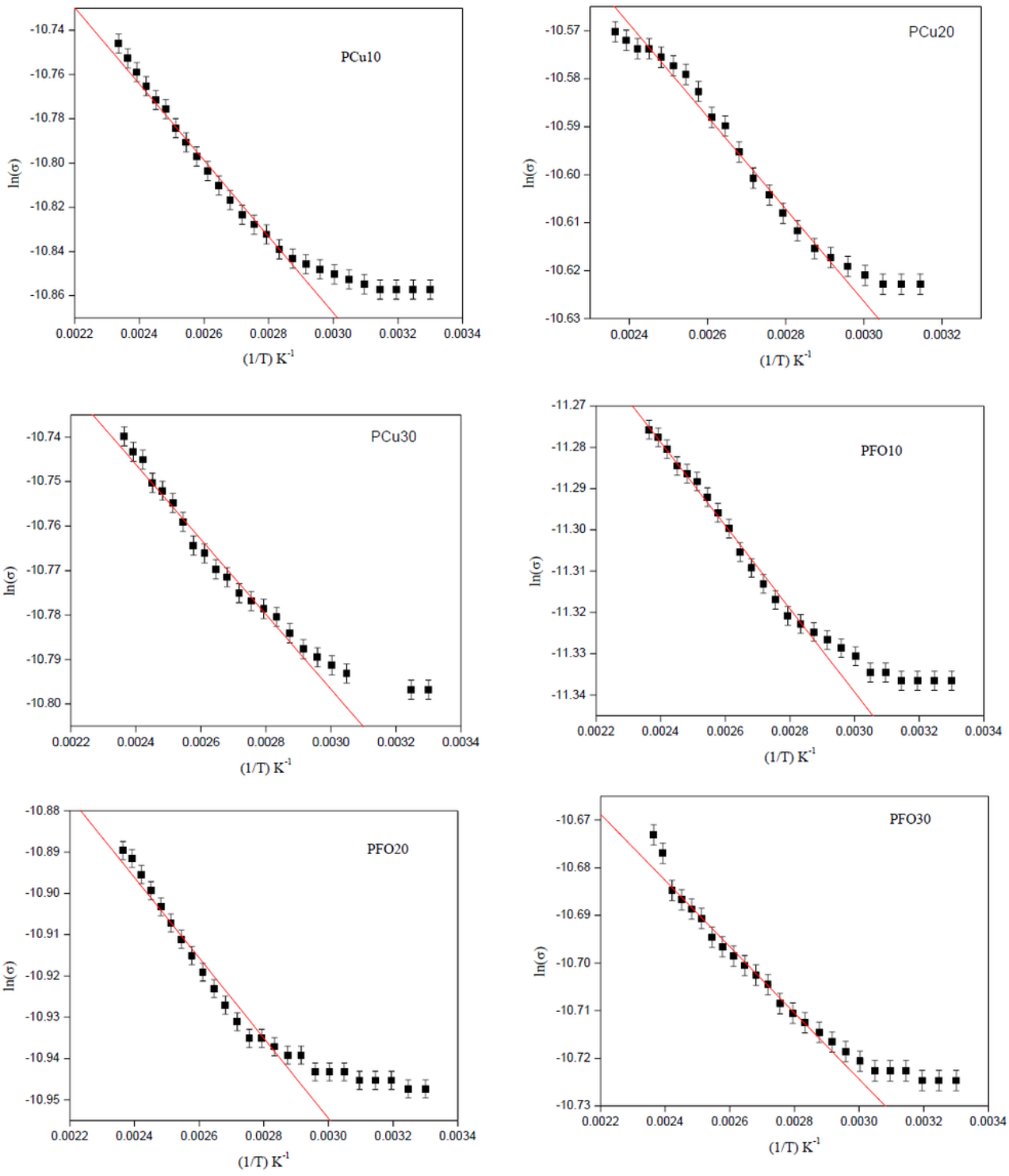

Figure 9

Plots of ln(σ) versus (1/T) for PCuO and PFO composites. Solid lines are the linear fits to data at high temperature.

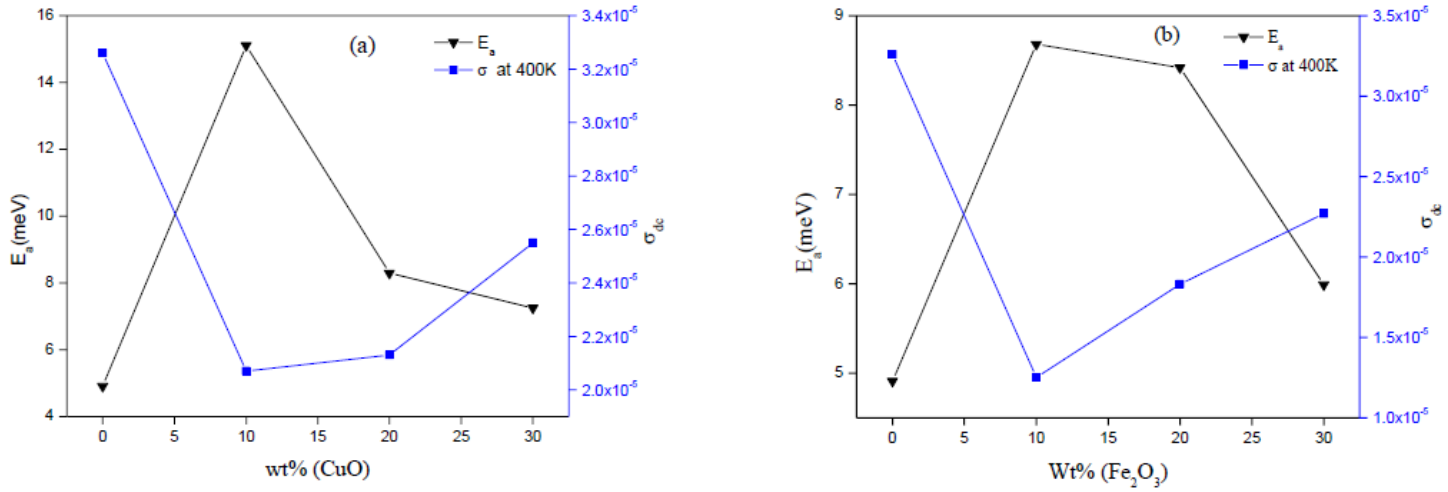

Figure 10

Plots of Ea and σ (400 K) versus (a) wt% of CuO and (b) wt% of Fe2O3 in their respective composites.